Available online at www.sciencedirect.com
SCIENCE DIRECT
C. R. Physique 7 (2006) 177–186
COMPTES RENDUS PHYSIQUE
http://france.elsevier.com/direct/COMREN/

High power fiber lasers and amplifiers/Lasers et amplificateurs à fibre de puissance

Performance and limitations of high brightness Er^{+3}–Yb^{3+} fiber sources

Guillaume Canat [a,*], Yves Jaouën [a,b], Jean-Claude Mollier [c]

[a] *ONERA, DOTA/SLS, 2, chemin de la Hunière, 91761 Palaiseau, France*
[b] *GET/Telecom Paris, CNRS UMR 5141, 46, rue Barrault, 75634 Paris, France*
[c] *Supaéro, 10, avenue Édouard-Belin, BP 54032, 31055 Toulouse cedex 4, France*

Available online 17 April 2006

Abstract

Recent development of fiber sources allows the generation of high peak power in the pulsed regime. Coherent LIDAR applications in the eye-safe window are designed with erbium–ytterbium fiber amplifiers. The main limitation to increase the optical power of narrow linewidth signals is the Stimulated Brillouin Scattering (SBS). A dynamic model for these fiber amplifiers is presented, and compared to the stationary model of the non-fluctuating localized source. Design rules are deduced for high brightness power fiber amplifiers. Enlarging the optical mode size increases the SBS threshold. However, fibers can guide several modes leading to a decrease in spatial quality. A detailed analysis of multimode propagation and refractive index profile inhomogeneities and their influence on beam quality has been conducted. Our numerical model has been applied to the design of an all-fiber MOPA source generating 100 μJ per pulse with 180 W peak power. ***To cite this article: G. Canat et al., C. R. Physique 7 (2006).***

Résumé

Performances et limitations des sources à fibre dopée Er^{3+}–Yb^{3+} de grande luminance. Le développement récent des sources à fibres dopées permet d'atteindre des puissances crêtes élevées en régime impulsionnel. Les applications LIDAR à détection hétérodyne et à sécurité oculaire utilisent des amplificateurs à fibres optiques dopées erbium–ytterbium pour l'amplification de signaux de faible largeur spectrale. La principale limitation pour la montée en puissance est la Diffusion Brillouin Stimulée (DBS). Un modèle dynamique d'amplificateurs est présenté et comparé au modèle stationnaire de la source localisée non fluctuante. Il en résulte des règles d'architecture pour la conception de sources de forte brillance. L'accroissement de la taille du mode optique permet d'augmenter le seuil de la puissance d'apparition du phénomène DBS. Les fibres dopées guident alors plusieurs modes ce qui conduit à une dégradation de la qualité spatiale du faisceau émis. Une analyse détaillée de l'impact de la propagation multimode et des inhomogénéités du profil d'indice sur la qualité du faisceau est menée. Une source laser entièrement à fibre, conçue à partir des modèles présentés, a permis la génération d'impulsions d'énergie 100 μJ et 180 W crête. ***Pour citer cet article : G. Canat et al., C. R. Physique 7 (2006).***

Keywords: Fiber amplifier; Double-clad fiber; Power amplifier; Erbium; Nonlinear effects; Modes

Mots-clés : Amplificateur à fibre ; Fibre à double gaine ; Amplificateur de puissance ; Erbium ; Effets non-linéaires ; Modes

* Corresponding author.
E-mail address: guillaume.canat@onera.fr (G. Canat).

1631-0705/$ – see front matter
doi:10.1016/j.crhy.2006.02.006

1. Introduction

Cladding-pumped rare-earth-doped fiber laser technologies have recently demonstrated their ability to compete with classical solid-state sources for many high power industrial applications such as marking, welding, micromachining, ... For these applications, power efficiency and brightness are essential. These criteria have driven major efforts on developing ytterbium (Yb) doped fiber lasers whose efficiency can reach 98% with $M^2 < 1.2$. For eye-safe LIDAR applications, pure erbium (Er) doped fibers and erbium–ytterbium (Er/Yb) codoped fibers are available. Although less efficient, these sources are still extremely compact and robust. They appear thus as good candidates for aeronautical and space applications. Recent developments have redefined the ranges of 'high power' fiber sources: a 1.36 kW SM CW Yb-fiber laser at 1 μm [1], 2 kW CW Yb-fiber laser with $M^2 < 1.2$ quality at 1 μm [2]. At 1.5 μm, 1.15 mJ in a pulsed Er/Yb fiber MOPA has recently been achieved [3].

A double-clad (DC) fiber is composed of two concentric waveguides: the outer one is strongly multimode and allows pump propagation. The inner waveguide is doped with the rare-earth ions. It is singlemode (SM) or slightly multimode (SMM). The DC fiber converts the poor beam-quality of high-power large-area pump diodes propagating in the inner cladding to laser light at another wavelength, guided in the active core. Assuming a uniform ray distribution by a proper choice of the inner cladding geometry, the effective pump absorption is reduced by the ratio of the core area to the inner-cladding one. The NA of Er fibers can be as low as 0.06 extending the range of singlemode operation of these fibers to large diameters. Er is prone to clustering and its absorption in the fiber core is limited to values below a few 10 dB/m. The pump absorption in DC pure Er fibers is then very low. They require extra length to absorb the pump power. Diffraction-limited laser diodes for core pumping doped fibers are limited to 1 W at most. High energy Er pulsed sources are thus limited to low pulse repetition rate below a few kHz (Table 1). In 1998, an Er LMA fiber delivered 500 μJ at 200 Hz giving 100 mW average power [4]. Due to the high absorption of Yb, Er/Yb DC fibers have enabled amplifier power scaling. These fibers also incorporate a large amount of phosphorous to improve Yb to Er transfer efficiency. However, the phosphorous codoping increases strongly the core refractive index. The numerical aperture of these fibers ranges from 0.11 to about 0.17. These fibers have thus a very limited range of single mode operation. Moreover, dopant migration and phosphorous evaporation during the perform sintering create a dip near the fiber center in the refractive index profile. This poor radial homogeneity enhances mode coupling and is detrimental to good beam quality. A 300 μJ MOPA source with $M^2 \sim 2.1$ [5] has been recently demonstrated. Energies up to 100 μJ have been obtained from an all-fiber MOPA with $M^2 \sim 1.4$ [6].

In fiber optics, the tight mode confinement leads to large intensities. Nonlinear effects have thus lower thresholds compared to bulk lasers. For spectroscopy and heterodyne LIDAR applications, amplification of a narrow linewidth ($\Delta\upsilon < 10$ MHz) signal is required. The spontaneous Brillouin spectrum (SBS) has a typical bandwidth $\Delta\upsilon_B \sim 30$ MHz in silica at 1.5 μm [9]. When amplifying narrow linewidth signal ($\Delta\upsilon \ll \Delta\upsilon_B$), SBS is then the nonlinear effect with the lowest threshold. This is especially true for pulsed signals: in a typical telecom amplifier with 10 m fiber length, the SBS threshold can be reached at only 10 W peak power. This nonlinear scattering is due to spontaneous acoustic waves in silica which act as moving gratings. The signal light is mainly backscattered into the Stokes wave downshifted by ∼11 GHz. When the signal is strong enough, the beating of the Stokes wave with the signal amplifies the acoustic waves, the scattering then becomes stimulated [10]. When the threshold is reached a large

Table 1
Main results for pulsed fiber sources at 1550 nm (FRL: Fiber ring laser; DFB–LD: DFB laser diode)

Tableau 1
Principaux résultats de sources laser pulsées à 1550 nm

Doping	λ (nm)	Energie (mJ)	Pulse duration (ns)	Laser oscillator	M^2	Repetition frequency	Team	Year
Er	1534	0.5	500	FRL	MM	200 Hz	ORC [7]	1998
Er	1555	0.45	80	DFB–LD		1 kHz	Coractive [4]	2004
Er/Yb	1536	0.29	100	DFB–LD	2.1	4 kHz	ORC [5]	2004
Er/Yb	1552	0.1	400	DFB–LD	1.4	15 kHz	ONERA/ Keopsys [6]	2005
Er/Yb	1535	1	88	DFB–LD	∼5	1 kHz	ORC [3]	2004
Er/Yb	1562	0.3	2	DFB–LD	1.7	2 kHz	Aculight [8]	2004

amount of power can be backscattered limiting the transmitted power. In fiber amplifiers, this backscattered light is amplified itself, leading to powerful spiking, potentially harmful for passive components such as optical isolators [11].

2. Modeling Stimulated Brillouin Scattering in double-clad pulsed amplifiers

We consider the interaction in a fiber amplifier between the signal wave with amplitude E_1, the Stokes wave with amplitude E_2 and the acoustic wave with normalized amplitude Q. The power P_i of the wave i is related to its amplitude E_i using the following conventions:

$$P_i = |E_i|^2 \tag{1}$$

We assume that the gain distribution $g(z,t)$ generated by the rare earth doping is the same for all optical waves. The amplifier equations then read [12]:

$$\frac{\partial E_1}{\partial z} + \frac{1}{v_s}\frac{\partial E_1}{\partial t} = \frac{g(z,t)}{2}E_1 - \frac{g_B}{2A_{\text{eff}}}QE_2 \tag{2a}$$

$$-\frac{\partial E_2}{\partial z} + \frac{1}{v_s}\frac{\partial E_2}{\partial t} = \frac{g(z,t)}{2}E_2 + \frac{g_B}{2A}Q^*E_1 \tag{2b}$$

$$\frac{\partial Q}{\partial t} + \frac{\Gamma_B}{2}Q = \frac{\Gamma_B}{2}E_1E_2^* + f \tag{2c}$$

$$\big\langle f(z,t)\big\rangle = 0 \tag{2d}$$

$$\big\langle f(z,t)f(z',t')\big\rangle = Q_0\delta(z-z')\delta(t-t') \tag{2e}$$

$$Q_0 = \frac{k_BTA\Gamma_B^2v_s}{4g_Bv_a} \tag{2f}$$

In these equations, v_s is the mode velocity; g is the amplifier local gain, g_B is the peak value of the Brillouin gain, A_{eff} is the mode effective area, Q is the normalized acoustic wave density, f is a Langevin force with white Gaussian process properties, $\Gamma_B = 2\pi\Delta\upsilon_B$ is the Brillouin linewidth, $v_a = 5960$ m/s is the acoustic velocity, $T = 300$ K is the temperature. We have measured, for a SMF28 fiber, $\Delta\upsilon_B = 30$ MHz at $\lambda_s = 1550$ nm and $\Delta\upsilon_B = 30$ MHz to 70 MHz for a doped fiber depending on the fiber doping characteristics [13]. The model (1)–(2f) is the so-called coherent model for SBS.

In (2a), (2b) the local gain $g(z,t)$ due to rare earth doping must be computed using a dynamical model which includes gain saturation by waves E_1 and E_2 [14]. During the propagation of a single pulse, the amplifier dynamic is dominated by gain saturation and an approximate expression for the gain variations can also be derived:

$$g(z,t) = 1 + \big(g(z,0) - 1\big)\exp\left(-\frac{E_{\text{out}}(z)}{E_{\text{sat}}}\right) \tag{3}$$

where E_{sat} is the saturation energy of the amplifier, $g(z,0)$ is the initial amplifier gain before pulse amplification, $E_{\text{out}}(z)$ is the energy flowing out of a small fiber slice between z and $z + \mathrm{d}z$.

This model thus includes stochastic initiation of the Brillouin scattering with finite bandwidth and gain saturation in the doped fiber. A simplified description of the SBS in the amplifier can be used when the phonon lifetime is very short compared to the pulse evolution allowing it to work with the steady-state equation of the acoustic waves. Eqs. (2a)–(2c) can then be transformed into:

$$\frac{\partial P_1}{\partial z} + \frac{1}{v_s}\frac{\partial P_1}{\partial t} = g(z,t)P_1 - \frac{g_B}{A_{\text{eff}}}P_1P_2 \tag{4a}$$

$$-\frac{\partial P_2}{\partial z} + \frac{1}{v_s}\frac{\partial P_2}{\partial t} = g(z,t)P_2 + \frac{g_B}{A}P_1P_2 \tag{4b}$$

$$P_2(L) = P_N \tag{4c}$$

where P_N is the equivalent noise power corresponding to spontaneous Stokes photons at $z = L$ which initiates the Stokes wave. Its value is adjusted in order to have the same average reflectivity $P_2(0)/P_1(0)$ as computed from (2a)–(2c) in the special case of passive fiber and continuous-wave input [10]:

$$P_N = \frac{kT\omega_s\Gamma L}{4A_{\text{eff}}\Omega_B} \tag{4d}$$

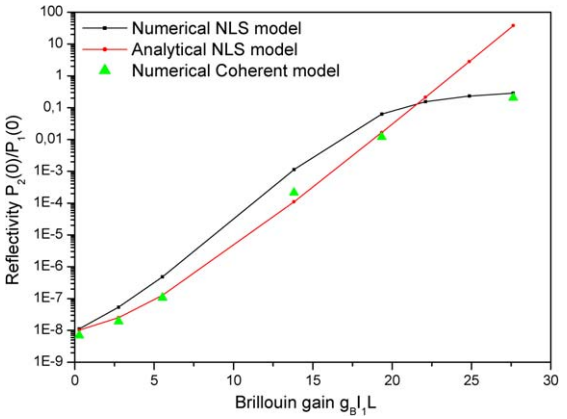

Fig. 1. Comparison of SBS reflectivity between the coherent and the NLS models for a continuous pump in a 10 m passive fiber.

Fig. 1. Comparaison des réflexions Stokes prévues par les modèles cohérents et NLS dans une fibre passive de 10 m pour une pompe continue.

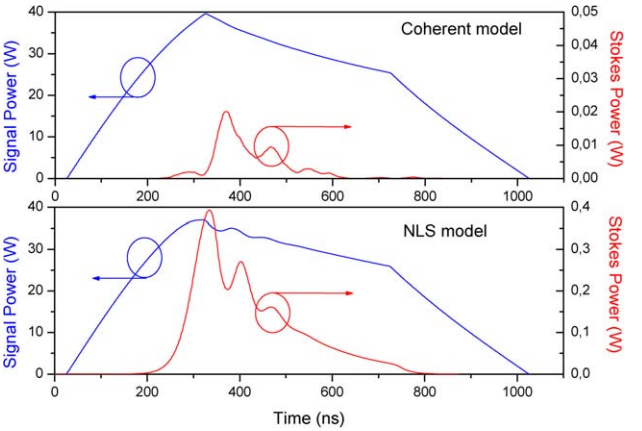

Fig. 2. Comparison between the coherent model and the NLS model for a 5 m long Er–Yb amplifier (core diameter 20 μm). The amplifier is counterpumped with 9 W.

Fig. 2. Comparaison entre les modèles cohérents et NLS pour un amplificateur Er–Yb de 5 m (diamètre de cœur 20 μm). L'amplificateur est pompé par une pompe de 9 W contrapropagative.

The set of equations (4a)–(4d) is called the non-fluctuating localized source SBS model (NLS).

In Fig. 1, the analytical NLS model is the solution of (4a)–(4d) assuming that the pump remains undepleted [10]. When the amplifier is operated in dynamic regime with gain saturation inducing pulse distortion, the fully dynamic model (2a)–(2c) must be used. Fig. 2 compares the propagation of a pulse with the steady-states model and the fully dynamic one with the same output peak power. These two sets of equations can be generalized to include second order Stokes wave contribution which can generate high peak power spikes potentially harmful for passive components such as optical isolators [11].

Using this model, it is now possible to look at the influence of the amplifier architecture on the SBS threshold. To get some insight into the amplifier properties, we transform Eqs. (4a)–(4d) assuming that the amplifier is operated in continuous-wave regime. Time derivatives in Eqs. (4a) and (4b) can then be dropped. Near threshold, the signal wave P_1 is undepleted. Integration then gives:

$$\begin{aligned} P_2(0) &= P_N \exp \int_0^L g(z)\,\mathrm{d}z \exp \frac{g_B}{A_{\text{eff}}} \int_0^L P_1(0) \left(\exp \int_0^z g(u)\,\mathrm{d}u \right) \mathrm{d}z \\ &= P_N \exp \int_0^L g(z)\,\mathrm{d}z \exp \frac{g_B L P_1(L)}{A_{\text{eff}}} \frac{\langle P_1 \rangle}{P_1(L)} \end{aligned} \tag{5}$$

In the last equation, we note $\langle P_1 \rangle$ the average power over the amplifier. Maximizing extractible power from the amplifier before the SBS onset thus leads to minimize the $r = \langle P_1 \rangle / P_1(L)$ requiring to have a large output power and a small average power. This simple rule allows to assess different configurations. First, let us note that if the amplifier gain G is assumed to be uniform along the fiber (5) reduces to

$$P_2(0) = P_N G \exp \frac{g_B L P_1(L)}{A_{\text{eff}}} \frac{1 - G^{-1}}{\ln G} \tag{6}$$

Defining the SBS threshold as $P_2(0)/P_1(0) = 10\%$ gives for a typical amplifier with $L = 5$ m, $A_{\text{eff}} = 72\ \mu\text{m}^2$, $g_B = 1.5 \times 10^{-11}\ \text{W}^{-1}\,\text{m}$, $G = 100$ and $P_1(L) = 54$ W. With the expression for r let us now consider the effect of the amplifier pumping configuration. In a copumped amplifier, the amplifier gain g is strong near the amplifier input whereas in a counterpumped amplifier it is stronger near the amplifier end. For the same output power, r is therefore larger for a copumped amplifier than for a counterpumped amplifier. The SBS threshold in the amplifier is thus larger in a counterpumped amplifier than in a copumped amplifier. To confirm this analysis, the coherent model has been

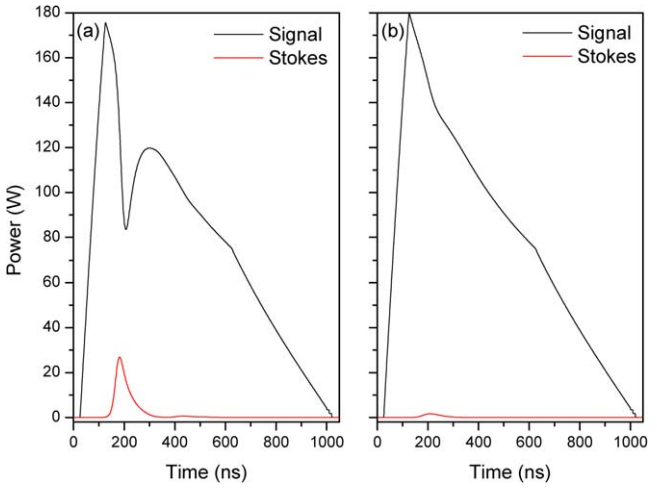

Fig. 3. Pulse shapes (coherent model) out of a 5 m fiber amplifier (a) copumping, (b) counterpumping.

Fig. 3. Forme des impulsions (modèle cohérent) en sortie d'un amplificateur à fibre de 5 m : (a) pompage copropagatif, (b) pompage contrapropagatif.

applied to a 20 μm core fiber amplifier whose length is 5 m pumped by 9 W. The amplification of 30 W peak power pulses at 20 kHz gives the results on Fig. 3. In the copumped configuration (a), the amplifier works beyond tbe SBS threshold leading to large pulse distortions. On the other hand, with the counterpumped configuration, the amplifier is just at the SBS threshold and almost no distortion is observed. We note that contrary to passive fibers, small Stokes fluctuations lead to large signal fluctuations due to the presence of gain in the fiber.

When designing high power fiber amplifiers the mode diameter must be increased to have larger SBS threshold. However, the input and pump powers required to saturate the amplifier also increase. As the core becomes larger, it guides more and more modes, decreasing the beam quality. There is thus a trade-off to find between high SBS power threshold, low saturation power and good beam quality. Modeling is thus helpful to estimate the performances of pulsed MOPA with a narrow linewidth oscillator.

3. Beam quality of large core fiber amplifiers

Making efficient Er/Yb doped fibers requires codoping with phosphorus [15]. It reduces the lifetime of level $^4I_{11/2}$ to a few microseconds which in turn allows it to have a good pump transfer efficiency in Er/Yb fibers. Alumina is also added to improve rare-earth solubility in silica. All these dopants result in a refractive index increase, leading to large numerical apertures. On the one hand, Yb doped fibers can now have NA as low as 0.06 and even singlemode PCF Yb doped LMA fibers have been demonstrated. On the other hand, Er/Yb doped fibers have larger NA (between 0.11 and 0.18). Fibers with core diameter in the range of 15–30 μm are thus multimode. Several ways have been suggested to operate these quasi-single fibers with singlemode beam quality. Fused tapers [16] allow the smooth enlargement of the fundamental mode of a standard singlemode fiber (∼10.6 μm diameter) larger mode size. This change must be adiabatic to avoid higher order modes.

Koplow et al. have showed that bending losses can be used as a distributed filter to suppress higher order modes in fibers with low numerical apertures [17]. Choosing the proper bending radius allows to give several 100 dB/m losses to higher order modes while the fundamental mode still propagates with negligible losses (Fig. 4). The larger bending losses of higher order modes are related to the fraction of power traveling into the cladding. However the same technique cannot be simply used with Er^{3+}–Yb^{3+} fibers due to their larger numerical aperture (Fig. 5). For instance, even for a fiber with NA 0.11, 100 dB/m losses on the LP_{11} mode require bending radius smaller than 20 mm. At the same time, bending losses for the fundamental mode smaller than 1 dB/m require bending radius larger than 20 mm.

Selective excitation of the fundamental mode can also achieve good beam quality. We have performed experiments and modeling showing the influence of injection conditions and core uniformity on the beam quality and stability. We assume that a single mode fiber with mode amplitude distribution ψ_0 is spliced to a multimode fiber guiding N modes with distribution ψ_k and propagation constant β_k, $k = 1, \ldots, N$. The modes are computed using a scalar model

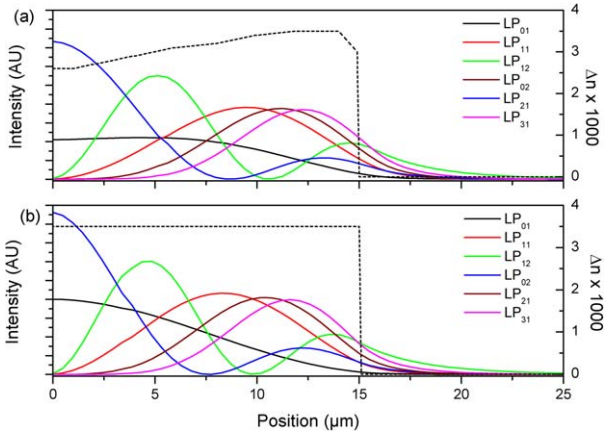

Fig. 4. LP_{lm} mode profiles for a 30 μm fiber NA 0.11: (a) typical real profile (with a central dip), (b) step index ideal profile.

Fig. 4. Répartition spatiale des modes LP_{lm} pour une fibre 30 μm et NA 0,11 : (a) profil réel (avec une dépression d'indice au centre), (b) profil à saut d'indice idéal.

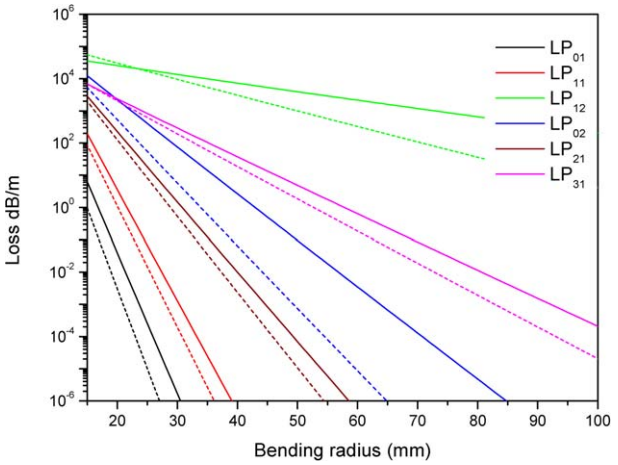

Fig. 5. Bending loss of the different LP_{lm} modes guided by the 30 μm fiber. Losses are computed assuming an ideal step index profile (dashed lines) and the real one (with central dip) (solid lines).

Fig. 5. Evolution, des pertes par courbure des différents modes LP guidés dans une fibres 30 μm. Les pertes sont déterminées pour un profil à saut d'indice idéal (pointillés) et un profil réel (avec trou central) (traits pleins).

ignoring polarization properties [18]. The coupled amplitude is $\tilde{\psi}_0$. The modal content of the downstream fiber is given by

$$\psi = \sum_{k=1}^{N} \langle \psi_k, \tilde{\psi}_0 \rangle \psi_k \tag{7}$$

where the scalar product between modes is

$$\langle \psi_k, \tilde{\psi}_0 \rangle = \iint_{\text{fiber}} \psi_k^*(r,\theta)\tilde{\psi}_0(r,\theta) r \, \mathrm{d}r \, \mathrm{d}\theta \tag{8}$$

If the splice process was perfect and quick enough (to prevent refractive index alteration), no tilt and no offset would be introduced and we would have: $\tilde{\psi}_0 = \psi_0$. Even with a perfect splice, as the fundamental mode of the multimode fiber has a different distribution from the input fiber, many modes with azimuthal order 0 can be excited with low amplitude coefficients. However, splices between different fibers especially when the cladding size is very different are prone to offset. The cleave themselves can have a small angle ($<1°$). All these imperfections will lead to coupling between the fundamental mode of the input fiber and modes with positive azimuthal order. We write the effect of the splice perturbations in terms of offset and tilt by operators O and T respectively. We thus have

$$\tilde{\psi}_0 = OT(\psi) \tag{9a}$$

with the small offset δr operator given by

$$O\psi(r) = \psi(r - \delta r) \tag{9b}$$

The tilt operator for a small tilt θ_x for the x axis and θ_y for the y axis is given by

$$T\psi(x,y) = \psi(x\cos\theta_x, y\cos\theta_y)\mathrm{e}^{jk(x\sin\theta_x + y\sin\theta_y)} \tag{9c}$$

Fig. 6 shows the relative amplitude coupled into the first modes of a 20 μm 0.11 NA fiber as a function of the mode mismatch assuming a tilt of 1° at the fiber junction. Even with a tilt as small as 1°, and perfect mode matching, up to 20% of the amplitude can be coupled into the LP_{11} mode. The excited modes will propagate according to

$$\psi(z) = \sum_{k=1}^{N} \langle \psi_k, \tilde{\psi}_0 \rangle \psi_k \mathrm{e}^{j\beta_k z} \tag{10}$$

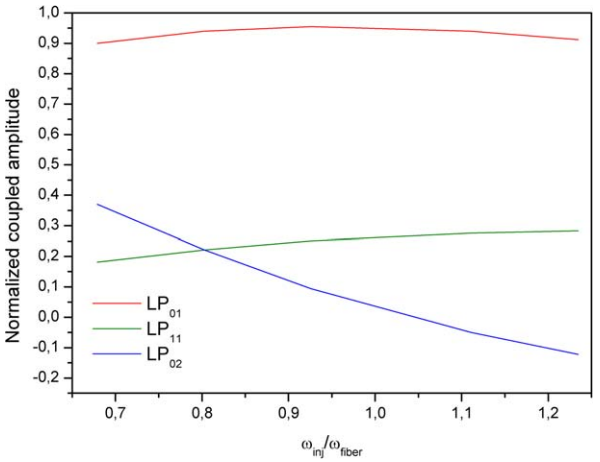

Fig. 6. Variation of the amplitude coupled into the first modes of the 20 μm fiber versus ratio between the mode sizes of the injection fiber and of the downstream fiber.

Fig. 6. Evolution de l'amplitude couplée dans les premiers modes d'une fibre de 20 μm fibre en fonction du rapport entre les tailles du mode injecté et du mode de la fibre aval.

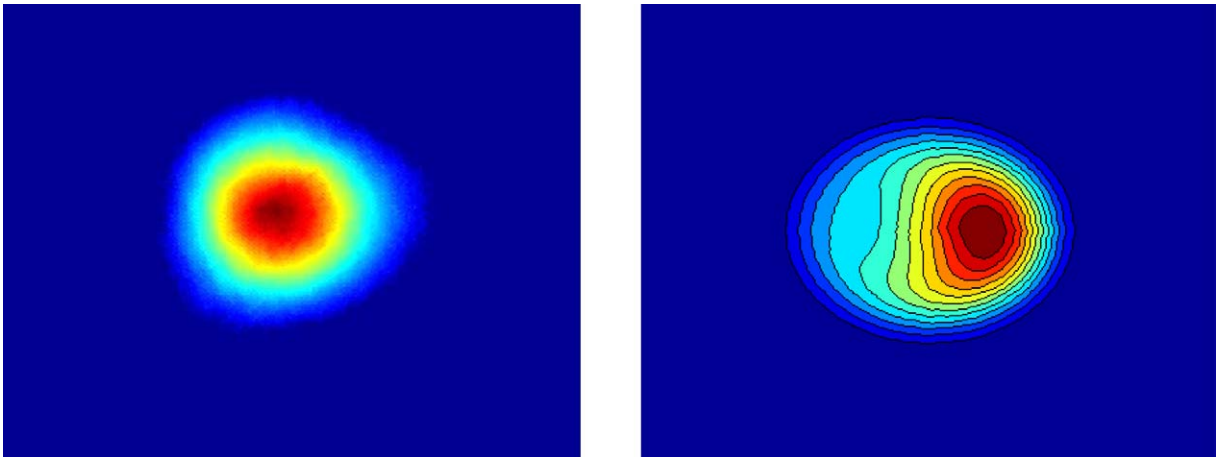

Fig. 7. Typical mode shape out of the 30 μm fiber showing a small amount of LP_{11} mode. Left: measurement using a CCD camera. Right: Modeling.

Fig. 7. Forme modale typique en sortie de la fibre 30 μm montrant une faible contribution du mode LP_{11}. Gauche : mesures avec une camera CCD, droite : modélisation.

The beam profile observed at the fiber output results from the interference of the different modes. As the propagation constants of these modes are pretty closed, the beam profile is quite sensitive to environmental conditions. For instance, for a 30 μm core with 0.11 NA the index difference between modes LP_{01} and LP_{11} is 5.56×10^{-4}.

Comparison of the actual beam profile at the fiber output and output of this simple modeling qualitatively explains the beam behavior (Fig. 7). This elongated bean shape of the beam is characteristic of the LP_{11}–LP_{01} interference. This interference can be a critical issue if the amplifier has to be used in systems. However it should be noted that very multimode fibers with 90 μm core diameter can lead to M^2 as good as 2.7 [19].

Another issue with Er^{3+}–Yb^{3+} fiber is phosphorous evaporation during the perform sintering. It results in a dip at the fiber center which degrades the core uniformity. The presence of this refractive index dip tends to reduce the effective index difference between the fundamental mode and higher order modes making mode coupling easier and reducing mode discrimination by bending. The shape of the fundamental mode differs from a Gaussian distribution: the mode vertex is flattened with a larger effective area (Fig. 8). When the core diameter is increased, the mode departs more and more from a Gaussian profile.

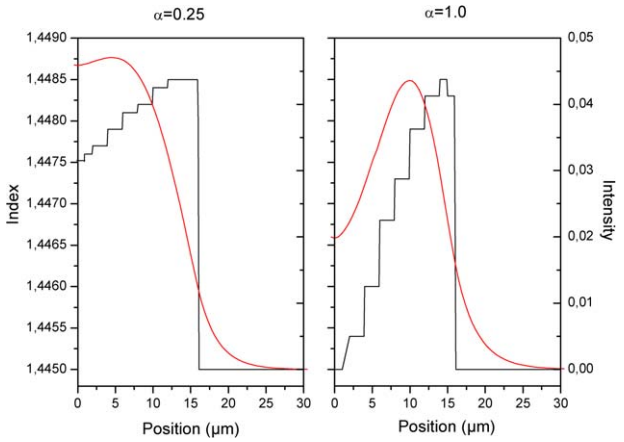

Fig. 8. Theoretical fundamental mode of the fiber for different dip deep.

Fig. 8. Forme du mode fondamental d'une fibre pour différentes dépressions d'indice.

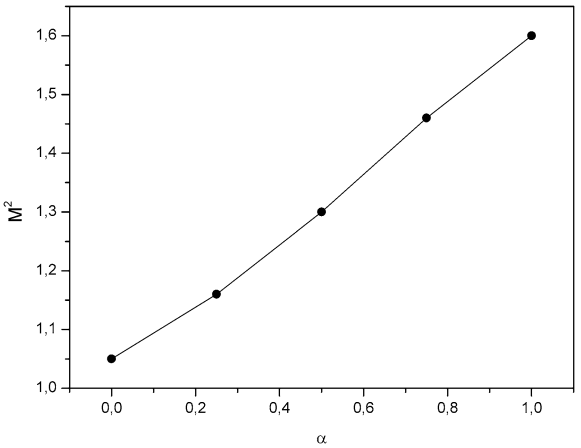

Fig. 9. Evolution of the M^2 parameter with the normalized index dip deep α.

Fig. 9. Variations du paramètre M^2 en fonction de la profondeur normalisée α de la dépression d'indice.

We have computed the mode fields for different value of the α parameter which is the ratio between the dip deep and the maximum index difference between core and cladding (Fig. 9). The M^2 parameter can be computed from mode size in real and transform space. In spite of the beam deformation, we have computed $M^2 \leqslant 1.5$ for fibers with core diameter below 50 μm.

4. Performance of a compact high brightness fiber amplifier

Balancing between the threshold for nonlinear effects and mode quality leads to carefully optimize the amplifier design: fiber diameters and length have to be chosen carefully. Using our modeling, we have designed and built a high brightness fiber source ($M^2 < 1.4$) delivering up to 180 W peak power and up to 100 μJ per pulse in collaboration with Keopsys.

We have built a three stage amplifier (Fig. 10). The first stage has a segmented pure Erbium fiber structure: two single mode different fibers have been concatenated with different Brillouin shifts and increasing core diameter. They are counterpumped by 250 mW singlemode pump diode. The second stage made of 2 m of Er–Yb codoped single mode DCF fiber with a 12 μm core diameter. The last stage is made of a 20 μm core ∼0.11 NA DCF fiber which guides 4 LP_{lm} modes. It is couterpumped by a fiber bundle. The output energy and average power are shown on Fig. 11. Pulse energy scale steadily as $1/PRF$ up to the point where SBS onset creates pulse distortion (Fig. 12).

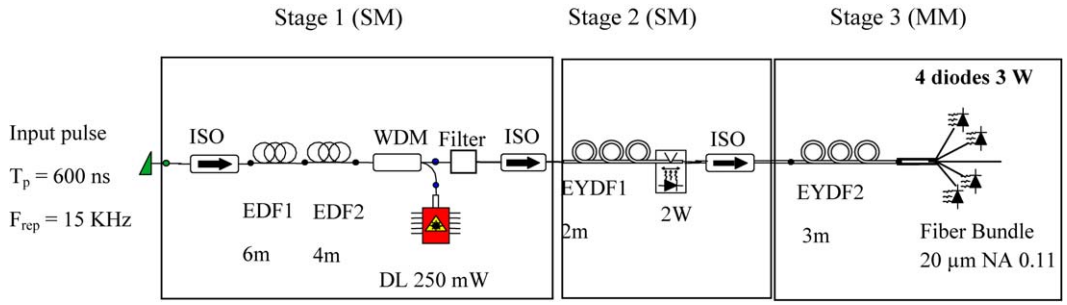

Fig. 10. The 100 μJ source architecture. The source is composed of 3 stages. The last one is multimode. (ISO: isolator; WDM: multiplexer; EDF: erbium doped fiber; EYDF: erbium–ytterbium doped fiber; DL: laser pump diode.)

Fig. 10. Architecture de la source 100 μJ. La source est composée de 3 stages. Le dernier étage est multimode. (ISO : isolateur ; WDM : multiplexeur ; EDF : fibre dopée erbium ; EYDF : fibre dopée erbium–ytterbium ; DL : diode laser de pompe.)

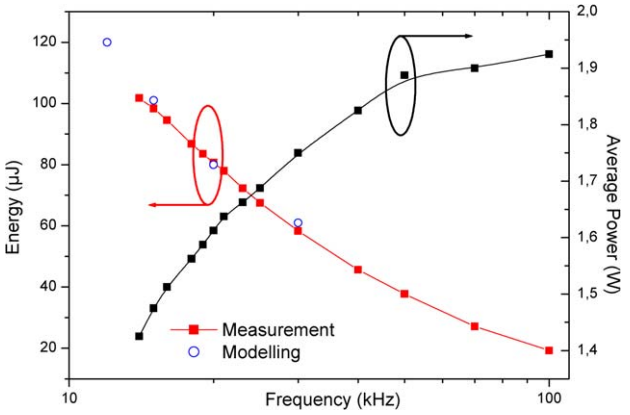

Fig. 11. Peak power as a function of the pulse repetition rate. Half width pulse duration is about 650 ns.

Fig. 11. Evolution de la puissance crête en fonction du taux de répétition. La durée des impulsions à mi-hauteur vaut 650 ns.

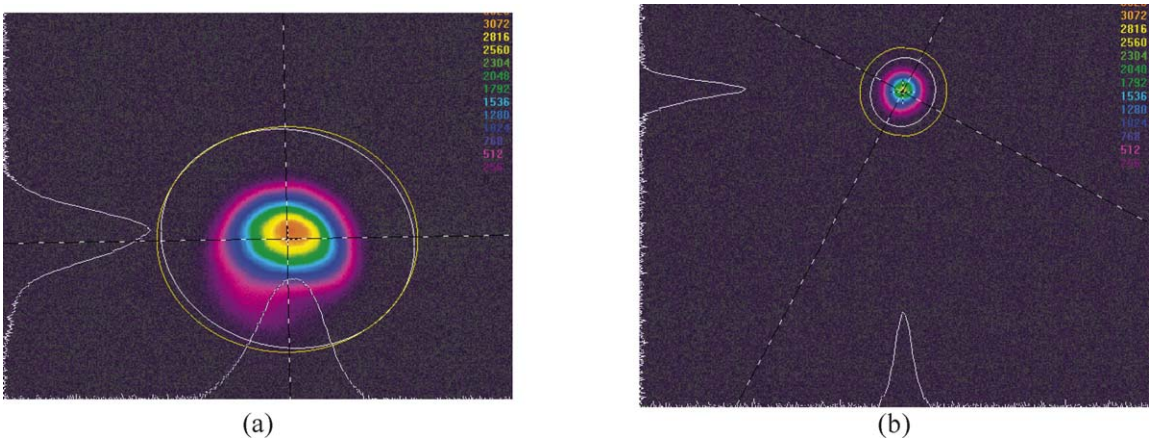

Fig. 12. Far field (a) and near field (b) beam shape at the amplifier output.

Fig. 12. Champ lointain (a) et champ proche (b) à la sortie de l'amplificateur.

5. Conclusion

In this article, a description of the limitations of erbium–ytterbium fiber amplifiers for coherent LIDAR applications has been presented. These amplifiers are mainly limited by Stimulated Brillouin Scattering for which a dynamic model has been presented. Counterpumping the amplifier leads to a larger threshold. Using large mode fibers also increases the threshold. However, the numerical aperture of erbium–ytterbium fiber is large. They thus guide several modes leading to a limited beam quality. A fiber source delivering 100 µJ with 180 W peak power has been designed and characterized. In order to get larger peak power and/or better beam quality, new concepts are required.

Acknowledgements

We would like to thank the company Keopsys for the interesting collaboration which allowed these source developments. This work was partially funded by the European project n° 12008 FIDELIO.

References

[1] Y. Jeong, J.K. Sahu, D.N. Payne, J. Nilsson, Ytterbium-doped large-core fiber laser with 1.36 kW continuous-wave output power, Opt. Express 12 (2004) 6088–6092.

[2] V.P. Gapontsev, D.V. Gapontsev, N.S. Platonov, et al., 2 kW CW ytterbium fiber laser with record diffraction limited brightness, in: CLEO Europe'05, paper CJ1-1-THU (2005).
[3] V. Philippov, J.K. Sahu, C. Codemard, et al., All-fiber 1.15 mJ pulsed eye-safe optical source, in: Proc. SPIE, vol. 5335, 2004.
[4] J.D. Minelly, V. Stasyuk, J.P. de Sandro, et al., Yb free high energy double-clad Er fiber amplifier, in: OAA'04, paper OPD P4, 2004.
[5] V. Philippov, C. Codemard, Y. Jeong, et al., High-energy in-fiber pulse amplification for coherent lidar applications, Opt. Lett. 29 (22) (2004).
[6] G. Canat, G. Loas, Y. Jaouën, et al., 100 μJ generation using a narrow linewidth Er^{3+}/Yb^{3+} doped fiber MOPA and its modeling, in: CLEO'05, paper JWB67, Baltimore, May 2005.
[7] H.L. Offerhaus, N.G. Broderick, D.J. Richardson, et al., High-energy single-transverse mode Q-switched fiber laser based on a multimode large-mode-area erbium-doped fiber, Opt. Lett. 23 (1998) 1683–1685.
[8] F. Di Teodoro, M. Savage-Leuchs, M. Norsen, High-power pulsed fibre source at 1567 nm, Electron. Lett. 40 (2004) 1525–1526.
[9] M. Niklès, L. Thévenaz, P.A. Robert, Brillouin gain spectrum characterization in single-mode optical fibers, J. Light. Technol. 15 (10) (1997) 1842–1851.
[10] S. Le Floch, P. Cambon, Theoretical evaluation of the Brillouin threshold and the steady-state Brillouin equations in standard single-mode optical fibers, J. Opt. Soc. Amer. A 20 (6) (2003) 1132–1137.
[11] G. Kulcsar, Y. Jaouën, G. Canat, et al., Multiple-Stokes stimulated Brillouin scattering generation in pulsed high-power double-cladding Er^{3+}–Yb^{3+} codoped fiber amplifier, IEEE Photon. Tech. Lett. 15 (6) (2003) 801–803.
[12] G.T. Moore, A model for diffraction-limited high-power multimode fiber amplifiers using seeded stimulated Brillouin scattering phase conjugation, IEEE J. Quant. Elec. 37 (2001) 781–789.
[13] G. Canat, A. Durécu, Y. Jaouën, S. Bordais, R. Lebref, Fiber composition influence on Spontaneous Brillouin Scattering properties in double-clad fiber amplifiers, CLEO06, submitted for publication.
[14] G. Canat, G.M. Williams, B. Cole, Y. Jaouën, et al., Dynamics of high power erbium–ytterbium fiber amplifiers, J. Opt. Soc. Amer. B 22 (11) (2005) 2308–2318.
[15] G.G. Vienne, J.E. Caplen, D. Liang, et al., Fabrication and characterization of Yb3+:Er3+ phosphosilicate fibers for lasers, J. Light. Technol. 16 (1998) 1990–2001.
[16] J.A. Alvarez-Chavez, A.B. Grudinin, J. Nilsson, P.W. Turner, W.A. Clarkson, Mode selection in high power cladding pumped fiber lasers with tapered sections, in: CLEO'99, paper CWE7, 1999, pp. 247–248.
[17] J.P. Koplow, D.A.V. Kliner, L. Goldberg, Single-mode operation of a coiled multimode fiber amplifier, Opt. Lett. 25 (2000) 442–445.
[18] J. Sakai, T. Kimura, Bending loss of propagation modes in arbitrary-index profile optical fibers, Appl. Opt. 17 (1978) 1499.
[19] J. Nilsson, J.K. Sahu, Y. Jeong, et al., High power fiber lasers, in: OFC'05, paperOTuF1, 2005.